Self-Consistent Mean Field Theory of the Microphases of Diblock Copolymers

J. D. Vavasour and M. D. Whitmore*

Department of Physics, Memorial University of Newfoundland, St. John's, Newfoundland, Canada A1B 3X7

Received March 17, 1992; Revised Manuscript Received June 10, 1992

ABSTRACT: Using self-consistent mean field theory, we have examined the phase behavior of diblock copolymers from the weak to the strong segregation regimes, considering spherical, cylindrical, and lamellar microphases. We showed that the phase diagram depends on three quantities: χr_C where r_C is an effective degree of polymerization, the relative volume fractions of each block, and $\epsilon = (\rho_{0B} b_B^2)/(\rho_{0A} b_A^2)$ where ρ_{0p} and b_p are the pure component density and Kuhn length for each block. For the model case of $\epsilon = 1$, this represents a generalization of the result found by Leibler for the weak segregation regime,[1] while the additional dependence on ϵ is consistent with the recent suggestion of Almdal et al.[2] We numerically calculated the phase diagram, domain sizes, and density profiles for $\epsilon = 1$. The phase diagram agrees with earlier work based on the narrow interphase approximation in the limit of strong segregation. It agrees with Leibler's RPA theory in weak segregation for symmetric copolymers, but there were significant differences for asymmetric copolymers even near the order–disorder transition. We also showed that if the domain spacing is expressed as $R \propto \chi^p Z^q$, then $q = p + 1/2$ for all three structures and in all segregation regimes, even though the values of p and q are larger in weak segregation than in strong. Finally, we related the polymer density profiles to the microphase behavior, in both regimes.

1. Introduction

It is well known that systems comprised of diblock A-*b*-B copolymers can undergo an order–disorder transition, which is frequently referred to as the microphase separation transition (MST), as well as a number of order–order transitions. At least four ordered microphases exist, of which three are the most widely studied.[3,4] They consist of alternating layers, which we denote L, cylinders on a hexagonal lattice, C, or spheres on a body-centered cubic lattice, S. As well, PS-*b*-PI exhibits a bicontinuous "double diamond" structure.[3,4]

Fully specifying such a system of monodisperse copolymers requires at least eight independent quantities: the total degree of polymerization Z of each molecule, the two Kuhn statistical lengths b_A and b_B and pure component densities ρ_{0A} and ρ_{0B}, the overall volume fraction of one component, f_A or $f_B = 1 - f_A$, the Flory interaction parameter χ, and the range of the interactions which is frequently taken to be zero. Nonetheless, the phase behavior is governed in large part by only three of them: Z, χ, and f_A. The MST occurs at a value of the product χZ which depends primarily on f_A, and the equilibrium microphase also depends primarily on only f_A. Consequently, the phase behavior is often summarized via a two-dimensional phase diagram showing the equilibrium microphase as a function of χZ and f_A. For each morphology, the domain size scales approximately as powers of χ and Z.

This picture has recently changed somewhat with the study of Almdal et al. of PEP-*b*-PEE copolymers with a fixed volume fraction of $f_{PEP} = 0.65$.[2] They discovered a sequence of four distinct phases as a function of temperature, including the disordered phase at the highest temperature and the lamellar phase at the lowest. Their results lead them to question the existence of a "universal" phase diagram depending on only χZ and f_A; instead, they suggested that it would also depend on what they called asymmetric block coil statistics, e.g., different Kuhn statistical lengths for each block.

Previous theoretical treatments of these systems have been for particular values of Kuhn lengths and pure component densities; in many cases model systems with $b_A = b_B$ and $\rho_{0A} = \rho_{0B}$ were assumed. One of the goals of this paper is examining the functional dependence of the phase diagram, and in fact we show that, within mean field theory, the microphase diagrams of all such systems an be expressed in terms of three quantities. Two of them are χr_C and f_A, where r_C is an effective degree of polymerization and is defined by eq 2 below. These reduce to χZ and f_A in the limit $\rho_{0A} = \rho_{0B}$ and $b_A = b_B$. The third quantity is $\epsilon = (\rho_{0B} b_B^2)/(\rho_{0A} b_A^2)$. It is characteristic of the differences in densities and Kuhn lengths of the two components, and incorporates differences in block coil statistics as suggested by Almdal et al.[2] It was also identified by Tanaka et al. as a characteristic determining the scattering from disordered copolymers.[5] Its value, which can be chosen to lie between 0 and 1, is system specific. For example, for PS-*b*-PBD or PS-*b*-PI we calculate $\epsilon \simeq 0.6$, using data for densities and Kuhn lengths taken from refs 6–9.

Most previous theories of these systems have focused on either the strong segregation regime, i.e., far from the MST, or the weak segregation regime, i.e., in some sense near it. For the strong segregation regime, Helfand and Wasserman[10] used their self-consistent mean field theory[11–16] and the narrow interphase approximation (NIA) to calculate the phase diagram for PS-*b*-PBD, finding phase boundaries separating the different microstructures which were almost independent of χZ; i.e., the equilibrium morphologies depended almost solely on the weight fractions. In particular, spheres were stable for PS weight fractions $w_{PS} \lesssim 0.1$ and $w_{PS} \gtrsim 0.85$, cylinders for $0.1 \lesssim w_{PS} \lesssim 0.3$ or $0.65 \lesssim w_{PS} \lesssim 0.85$, and layers for $0.3 \lesssim w_{PS} \lesssim 0.65$. This was in general accord with what is observed. In the context of the current paper, we associate the asymmetry of this phase diagram with the fact that $\epsilon \neq 1$.

The weak segregation regime has been treated for model systems with $\epsilon = 1$ by Leibler,[1] Fredrickson and Helfand,[17] and Mayes and Olvera de la Cruz.[18–20] Common features of these calculations are the requirement that the ensemble average density variations be small and can be described by functions of at most a few wavenumbers, and the use of fourth-order expansions for the free energy of each microphase relative to the homogeneous phase. These

0024-9297/92/2225-5477$03.00/0

approaches all predicted phase diagrams near the MST which were qualitatively different from those predicted for the strong segregation regime, with curved microphase boundaries. Leibler's RPA theory predicted that for any asymmetric copolymers, $f_A \neq f_B$, then as a function of increasing χZ the first equilibrium microphase consisted of spheres, followed by transitions first to cylinders and then to lamellae. A sequence of phases for fixed f_A is qualitatively consistent with the observations of Almdal et al.[2] However, the sequence was predicted to occur for any $f_A \neq 0.5$; the region of cylinders was rather small, and that of spheres very small. The theory of Fredrickson and Helfand,[17] which was extended by Mayes and Olvera de la Cruz,[20] incorporated fluctuation effects. They found that Z enters as an additional independent variable controlling the microphase behavior. For finite Z small "windows" on the phase diagram opened up, through which the system could pass directly from the homogeneous to the lamellar or the cylindrical phases. However, as these windows appeared, the S region on the phase diagram diminished, disappearing for $Z \lesssim 10^4$.

There have also been recent treatments of the microphase diagram of copolymer/neutral solvent blends. Birshtein and Zhulina applied scaling theory to model copolymer/solvent blends in the strong segregation regime.[21] For the case of copolymer/neutral solvents they found, in this limit, that the equilibrium morphology was independent of overall concentrations, and unaffected by the swelling. The L ↔ C microphase boundaries occurred at $f_A \simeq 0.28$ and 0.72, and the C ↔ S boundaries at $f_A \simeq 0.13$ and 0.87 which, allowing for the asymmetry in PS-*b*-PBD, were in good agreement with the results of Helfand and Wasserman. In two recent papers, we applied the mean field self-consistent formalism developed by Hong and Noolandi[22-25] to this case, numerically solving the self-consistent field equations, with no a priori assumption about the shape of the equilibrium density profiles, without assuming the NIA, and without truncating the free energy expression to fourth order. In one paper,[26] we calculated a number of microphase diagrams for model systems, finding in particular that they could be illustrated in terms of two quantities. One is $\bar{\phi}_c \chi Z$ where $\bar{\phi}_c$ is the overall copolymer volume fraction, and the other is f_A as defined above. When expressed in these terms, the five phase diagrams which we calculated turned out to be very similar. To this extent, the dominant effect of the solvent on the microphase diagram was simply to reduce the interaction parameter to an effective value, $\chi_{eff} = \bar{\phi}_c \chi$, i.e., the dilution approximation. The results suggested that the case of neat copolymers would correspond to the limiting case of $\bar{\phi}_c = 1$. In the other paper,[27] we concentrated on the lamellar structure, examining the variation of the layer thickness and density profiles with the overall concentrations, the copolymer degree of polymerization, and the A–B interaction parameter.

The first goals of this paper are examining the functional dependence of the microphase diagram of diblock copolymers, and calculating it for a model system using numerical solutions to the self-consistent equations of mean field theory. Second, we calculate the dependence of the domain sizes on Z and χ for different microstructures. Finally, we examine the density profiles both near the MST and in the strong segregation regime. The three common structures L, C, and S are examined, and the effects of a finite range for the interactions are considered briefly. Detailed comparisons are made with previous results for copolymers and, in some cases, copolymer/solvent blends.

2. Formalism and Procedure

The formalism derived here is an extension of that presented in ref 28 with modifications introduced as in ref 29. The procedures for treating periodic microphases follow refs 26 and 27.

We need to calculate the equilibrium morphology and corresponding domain size, density profiles, and free energy for a system of monodisperse copolymers with total degree of polymerization Z and block degrees of polymerization Z_A and $Z_B = Z - Z_A$. We associated with each block p, p = A, B, a pure component density, ρ_{0p}, and a Kuhn statistical length, b_p. The overall volume fraction of block p was

$$f_p = r_p/r_C \equiv \bar{\phi}_p \tag{1}$$

where

$$r_p = \rho_0 Z_p/\rho_{0p}$$

$$r_C = r_A + r_B \tag{2}$$

ρ_0 is the reference density used in defining the Flory χ parameter, and r_C is sometimes referred to as an effective degree of polymerization.

For each microphase considered, S, C, or L, the system was assumed to form an infinite periodic structure, described by a set of lattice vectors $\mathbf{R}_n$ and an associated unit cell of volume Ω. We represented each molecule by a flexible space curve, expressing the partition function as a functional integral incorporating a Dirac δ function to ensure incompressibility. This integral was approximated by the saddle point method, resulting in a mean field approximation for the equilibrium density distributions and free energy. We needed to solve modified diffusion equations for propagators

$$\left[-\frac{b_p^2}{6}\nabla^2 + \omega_p(\mathbf{r})\right] Q_p(\mathbf{r}, \tau|\mathbf{r}') = -\frac{\partial}{\partial \tau} Q_p(\mathbf{r}, \tau|\mathbf{r}') \tag{3}$$

subject to periodic boundary conditions

$$Q_p(\mathbf{r}, 0|\mathbf{r}') = \sum_n \delta(\mathbf{r} - \mathbf{r}' - \mathbf{R}_n) \tag{4}$$

It was sufficient to solve for Q_p in one unit cell. The local volume fractions were calculated from the solutions via

$$\phi_A(\mathbf{r}) = \frac{\bar{\phi}_A V}{Z_A Q_C}\int_0^{Z_A} d\tau\, q_A(\mathbf{r}, \tau)\int_\Omega d\mathbf{r}'\, Q_A(\mathbf{r}, Z_A - \tau|\mathbf{r}')\, q_B(\mathbf{r}', Z_B) \tag{5}$$

for component A, and a corresponding expression for $\phi_B(\mathbf{r})$. In this expression

$$q_p(\mathbf{r}, \tau) = \int_\Omega d\mathbf{r}'\, Q_p(\mathbf{r}, \tau|\mathbf{r}') \tag{6}$$

and

$$\frac{Q_C}{V} = \frac{1}{\Omega}\int_\Omega d\mathbf{r}\, q_A(\mathbf{r}, Z_A)\, q_B(\mathbf{r}, Z_B) \tag{7}$$

The potentials appearing in the diffusion equation can be expressed as

$$\omega_A(\mathbf{r}) = \frac{\rho_0}{\rho_{0A}}\left[\chi\left(\phi_B(\mathbf{r}) - \bar{\phi}_B + \frac{\sigma^2}{6}(\nabla^2\phi_B(\mathbf{r}) - \overline{\nabla^2\phi_B})\right) + \frac{\eta(\mathbf{r})}{\rho_0}\right] \tag{8}$$

$$\omega_B(\mathbf{r}) = \frac{\rho_0}{\rho_{0B}}\left[\chi\left(\phi_A(\mathbf{r}) - \bar{\phi}_A + \frac{\sigma^2}{6}(\nabla^2\phi_A(\mathbf{r}) - \overline{\nabla^2\phi_A})\right) + \frac{\eta(\mathbf{r})}{\rho_0}\right] \tag{9}$$

where σ is a measure of the range of the interactions,[23] $\eta(\mathbf{r})$ is the Lagrange multiplier field associated with the incompressibility, and $\phi_p(\mathbf{r})$ are the local volume fractions which satisfy

$$\phi_A(\mathbf{r}) + \phi_B(\mathbf{r}) = 1 \tag{10}$$

everywhere. In this paper we use $\sigma = 0$, and drop it from the rest of the formalism.

The saddle point approximation for the free energy can be written as

$$F = F_{hom} + \Delta F \tag{11}$$

where F_{hom} is the free energy of a homogeneous bulk phase of the system. Dividing by the total volume V and the reference density ρ_0, the reduced free energy density ΔF can be expressed as

$$\frac{\Delta F}{\rho_0 k_B T V} = \frac{1}{\Omega}\int_\Omega d\mathbf{r}\left\{\chi[\phi_A(\mathbf{r})\,\phi_B(\mathbf{r}) - \bar{\phi}_A\bar{\phi}_B] - \frac{\rho_{0A}}{\rho_0}\omega_A(\mathbf{r})\,\phi_A(\mathbf{r}) - \frac{\rho_{0B}}{\rho_0}\omega_B(\mathbf{r})\,\phi_B(\mathbf{r})\right\} - \frac{1}{r_C}\ln\left(\frac{Q_C}{V}\right) \tag{12}$$

For a given structure and an assumed lattice constant, e.g., domain spacing, eqs 1–10 constitute a self-consistent problem. When it was solved, the reduced free energy per unit volume, relative to a uniform melt, was calculated via eq 12.

In earlier work on copolymer/solvent blends, $\eta(\mathbf{r})$ was related directly to the solvent density at $\mathbf{r}$.[22,23,26-28] In the problem of interest in this paper, as in that of Helfand and co-workers,[10-16] there is no solvent and a different method was needed to find $\eta(\mathbf{r})$. Our approach, which is similar to that used in refs 10–16, used the implication of eqs 8–10 that

$$\eta(\mathbf{r}) = \frac{\rho_{0A}\omega_A(\mathbf{r}) + \rho_{0B}\omega_B(\mathbf{r})}{2} \tag{13}$$

For each calculation, we started with initial guesses for $\eta^{(0)}(\mathbf{r})$ and each $\phi_p^{(0)}(\mathbf{r})$, usually simply using $\eta^{(0)}(\mathbf{r}) = 0$ and hyperbolic tangents for the $\phi_p^{(0)}(\mathbf{r})$. From these we evaluated $\omega_A^{(0)}(\mathbf{r})$ and $\omega_B^{(0)}(\mathbf{r})$ from eqs 8 and 9. We next used these in the diffusion equation to calculate the propagators, and from these calculated new local volume fractions using eq 5 for $\phi_A^{(1)}(\mathbf{r})$ and a similar convolution for $\phi_B^{(1)}(\mathbf{r})$. A new $\eta(\mathbf{r})$ was calculated from

$$\eta^{(1)}(\mathbf{r}) = \frac{\rho_{0A}\omega_A{}^{(0)}(\mathbf{r}) + \rho_{0B}\omega_B{}^{(0)}(\mathbf{r})}{2} \tag{14}$$

At this point, we had new fields $\eta^{(1)}(\mathbf{r})$ and $\phi_p^{(1)}(\mathbf{r})$. New potentials $w_p(\mathbf{r})$ were calculated from these via eqs 8 and 9. In general, the potentials actually used in successive iterations were calculated from linear combinations of these newly generated potentials and ones from previous iterations, using the secant method.

As described more fully in ref 26, for each system we performed a series of self-consistent calculations to determine the equilibrium microstructure, L, C, or S, and corresponding lattice parameters and free energy, ΔF_L, ΔF_C, or ΔF_S. For example, in order to find a point on the L ↔ C phase boundary, we fixed χ and r_C and calculated ΔF_L and ΔF_C as functions of f_A, in each case minimizing them with respect to the lattice parameters. The phase boundary corresponds to the point at which $\Delta F_L = \Delta F_C$. As discussed in the next section, a slightly different procedure was used to find the MST of perfectly symmetric copolymers.

In the layered structure, the problem is one-dimensional and the lattice parameter coincides with the repeat distance, or layer thickness, d; hence, we needed to solve for the functions $Q_p(x, \tau|x')$ and $q_p(x, \tau)$ in the spatial interval $[0, d]$ and for $\tau\epsilon[0, Z_p]$. For the other structures, we approximated the unit cell by a cylinder or sphere which contains one domain, with its radius denoted by R. Thus, we ignored detailed structural effects; for example, we did not distinguish between a body-centered cubic or a face-centered cubic array of spheres. As in ref 26, we estimated that the phase boundaries (within the limitations of the model) were located to within $\Delta f_A \simeq \pm 0.001$, except in a few cases very near the MST where the precision was about ±0.003.

3. Results

3.1. Phase Diagrams. As we show in Appendix I, if the interactions are modeled using just a Flory parameter, i.e., $\sigma = 0$, then the equilibrium phase is determined by three quantities, which we can take to be χr_C, f_A, and the ratio $\epsilon = (\rho_{0B}b_B^2)/(\rho_{0A}b_A^2)$. This can be understood physically as follows. On one hand, it is clear that the equilibrium morphology should depend on the relative volume fractions f_A and f_B, which satisfy

$$\frac{f_A}{f_B} = \frac{Z_A\rho_{0B}}{Z_B\rho_{0A}} \tag{15}$$

On the other hand, relative domain sizes and hence the equilibrium morphology should be controlled at least in part by the unperturbed radii of gyration for the two blocks. They satisfy

$$\frac{R_{A,g}{}^2}{R_{B,g}{}^2} = \frac{Z_A b_A{}^2}{Z_B b_B{}^2} \tag{16}$$

The quantity ϵ is equivalent to the ratio

$$\epsilon = (f_A/f_B)/(R_{A,g}{}^2/R_{B,g}{}^2) \tag{17}$$

and is a measure of the dissimilarity between these factors. The case $\epsilon = 1$ corresponds to

$$\frac{f_A}{f_B} = \frac{Z_A b_A{}^2}{Z_B b_B{}^2} \tag{18}$$

The choice of $\rho_{0A} = \rho_{0B}$ and $b_A = b_B$, which was used in most previous theoretical treatments and which we use for the numerical work of this paper, is one of these cases. It also implies that $r_C = Z$ and $f_A = Z_A/Z$, but the results presented here would apply to other systems with $\epsilon = 1$ simply through the replacement of Z with r_C.

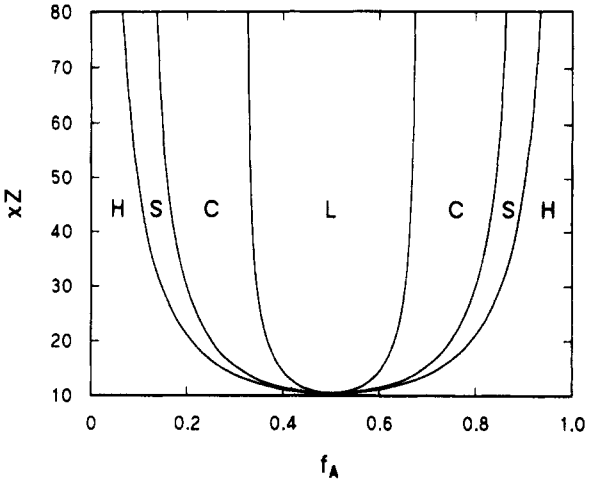

Figure 1. Calculated phase diagrams for model copolymers with $\rho_{0A} = \rho_{0B}$ and $b_A = b_B$, as a function of the volume fraction of the A block of the copolymers, f_A, and χZ where χ is the Flory interaction parameter and Z is the total degree of polymerization. The diagram would apply to other copolymers with $\rho_{0A}b_A^2 = \rho_{0B}b_B^2$, but with the vertical axis relabeled χr_C with r_C as defined by eq 2.

Figure 1 shows the calculated phase diagram for these systems, ranging from the vicinity of the MST to the strong segregation regime with $\chi Z = 80$, and Figure 2 compares them directly with earlier mean field calculations. In making these comparisons, it is useful to recall that the phase diagrams are symmetric about $f_A = 0.5$. For convenience, Figure 2 explicitly shows the Leibler result for $f_A < 0.5$ and the NIA result for $f_A > 0.5$, but each one could be extended into the other half of the diagram.

In most cases, the phase boundaries were calculated as described in the previous section. The region near the MST for $f_A = 0.5$ was explored through a series of calculations in which we fixed f_A at 0.5, and calculated ΔF for each structure, varying Z or χ independently. In all such calculations, ΔF_L, ΔF_C, and ΔF_S all reached zero at values of χZ which agreed with each other to within the numerical accuracy of about ±0.004, with the lamellar

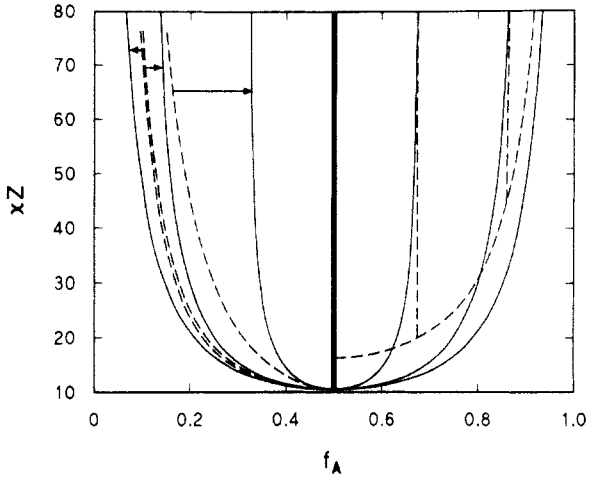

Figure 2. Comparison with earlier work. The solid curves are the present calculation, repeating Figure 1. For $f_A < 0.5$, the dashed curves are calculated using the theory of Leibler,[1] with the arrows indicating the corresponding phase boundaries in the current work. For $f_A > 0.5$, the dashed curves are calculated using the theory of Helfand and co-workers.[10]

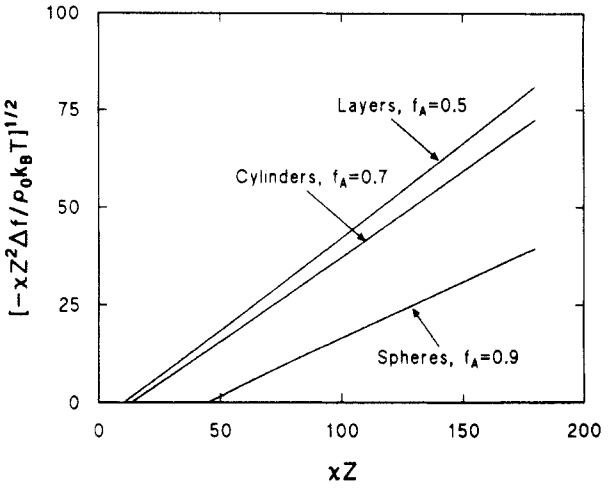

Figure 3. Scaled free energy density for three systems in different morphologies, as labeled.

morphology consistently having a slightly lower free energy away from this point. Thus, the calculations are consistent with the lamellae being the only equilibrium morphology for perfectly symmetric copolymers, with all phase boundaries converging at $f_A = 0.5$ and $\chi Z = 10.5$.

Moving away from $f_A = 0.5$, the phase boundaries begin to turn upward, and the MST is a first-order transition to spheres. For all fixed $f_A \neq 0.5$ but lying between about 0.33 and 0.67, there is predicted to be a sequence of phases H → S → C → L, occurring with increasing χZ. In the strong segregation regime, the microphase boundaries are nearly vertical, i.e., only weakly dependent on χZ, reaching $f_A \simeq 0.67$ (L ↔ C transition), and $f_A \simeq 0.85$ (C ↔ S transition) for $\chi Z = 80$.

As illustrated in the left-hand panel of Figure 2, near the MST these results agree qualitatively with those of the Leibler theory, with the agreement becoming quantitative as $f_A \to 0.5$. However, differences begin to develop with increasing asymmetry, even near the MST. First, for a given f_A the MST occurs at smaller values of χZ. For modest asymmetry, the shift is very small. For example, for $f_A = 0.3$ the MST is shifted from the Leibler prediction of $\chi Z \simeq 14$ to $\chi Z \simeq 13$, and for $f_A = 0.2$ from $\chi Z \simeq 24$ to $\chi Z \simeq 21$. However, for $f_A = 0.15$ the shift is from $\chi Z \simeq 38$ to $\chi Z \simeq 30$, and for $f_A = 0.1$ from $\chi Z \simeq 80$ to $\chi Z \simeq 48$. Furthermore, for values of χZ on the order of 15 and larger, the microphase boundaries turn upward more quickly, resulting in much broader C and S regions and a correspondingly narrower L region than predicted in any of the weak segregation regime theories. For example, at $\chi Z = 50$, the L ↔ C transition is shifted from the Leibler value of $f_A \simeq 0.2$ to $f_A \simeq 0.33$, the C ↔ S transition from $f_A \simeq 0.13$ to $f_A \simeq 0.16$, and the MST from $f_A \simeq 0.12$ to $f_A \simeq 0.1$. These result in a narrowing of the L region by a factor of almost 2, and broadening of the C and S regions by factors of about 2.5 and 5, respectively. The relatively wide S region for asymmetric copolymers constitutes a difference from all previous weak segregation theories even very near the MST.

In the strong segregation regime, the results are consistent with those of the NIA of Helfand and Wasserman[10] and Birshtein and Zhulina.[21] A direct comparison with the former is shown in the right panel of Figure 2, which we calculated for this system using the program published in ref 10. The L ↔ C boundaries have reached agreement by $\chi Z \simeq 50$ and the C ↔ S boundaries by $\chi Z \simeq 70$. The S ↔ H have not merged by this point, but are approaching one another. Note, however, that the predicted S regions are quite different in the region $\chi Z \simeq 50$. The NIA approximation predicts that this region thins and disappears near $\chi Z \simeq 45$, whereas the current work predicts a thickness of $\Delta f_A \simeq 0.1$ near here.

The structure of the microphase diagram is very similar to what we found for copolymer/neutral solvent blends, with the primary difference being the correspondence of χZ for the present case with $\bar{\phi}_c \chi Z$ for the blends.[26] It can be shown analytically that the small differences between the copolymer and the blend cases which do appear, assuming $\sigma = 0$ for both cases, are due to the small inhomogeneities in the solvent (and total copolymer density) profile.

3.2. Free Energy. We show in Appendix I that, for each structure, the minimized free energy has a relatively simple functional dependence which can be expressed as

$$\frac{\Delta F}{\rho_0 k_B T V} \propto \frac{1}{Z} \tilde{F}(\chi Z, f_A) \tag{19}$$

Figure 3 exhibits rescaled calculations of the free energy density ($\Delta f = \Delta F/V$) for three cases, corresponding to symmetric, modestly asymmetric ($f_A = 0.7$), and highly asymmetric ($f_A = 0.9$) copolymers in the lamellar, cylindrical, and spherical structures, respectively. In each case, the free energy can be expressed to leading order as

$$\frac{\Delta F}{\rho_0 k_B T V} \propto -\frac{1}{Z}\frac{1}{\chi Z}(\chi Z - \alpha)^2 \tag{20}$$

where both the proportionality constant and the intercept α depended on the structure and f_A. (For the case of spheres, and for layers if $f_A = 0.5$, α corresponds to the value of χZ at the MST). This is the same as was found earlier for the free energy of the lamellar structure in copolymer/neutral solvent blends.[27] The degree to which the leading term, i.e., expression 20, dominates is reflected in the degree to which the curves in this figure are straight lines.

3.3. Domain Sizes. Figures 4–6 show the calculated equilibrium domain sizes for the three structures as functions of Z for fixed χ, and as functions of χ for fixed Z. All these calculations correspond to vertical paths through the phase diagram, Figure 1. In all cases, the dependences are nearly power laws but with values of the exponents which in some cases vary slightly. This behavior

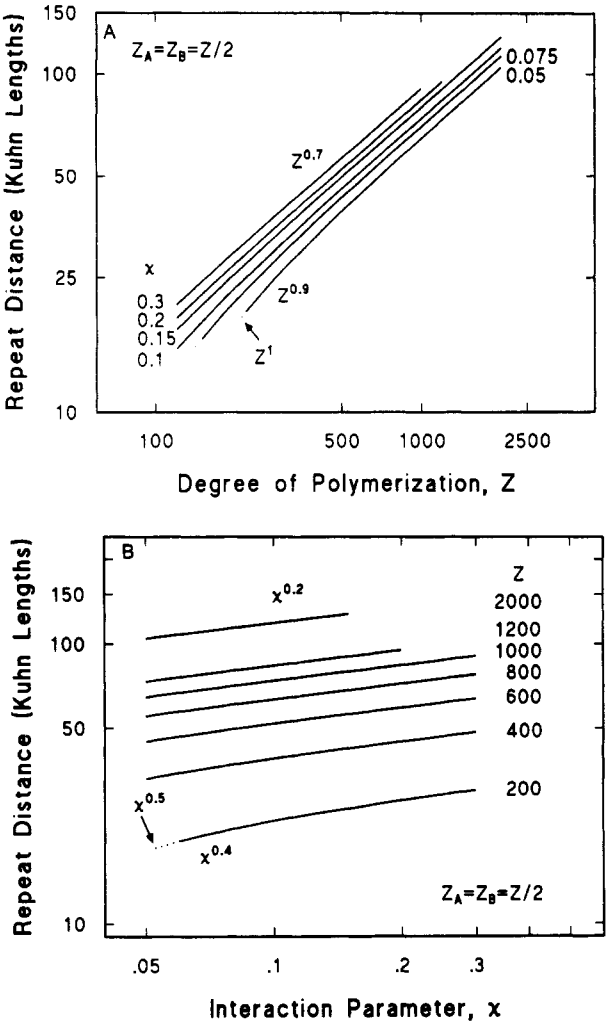

Figure 4. (A) Equilibrium repeat distance d as a function of the copolymer degree of polymerization Z, for symmetric copolymers with $Z_A = Z_B$, for the lamellar structure. (B) Equilibrium repeat distance d as a function of the interaction parameter χ for the same system. The solid lines represent values calculated from the full self-consistent theory, and terminate on the left before the MST is reached. The dotted line segment represents an extrapolation to the value at the MST predicted by Leibler's RPA theory.[1]

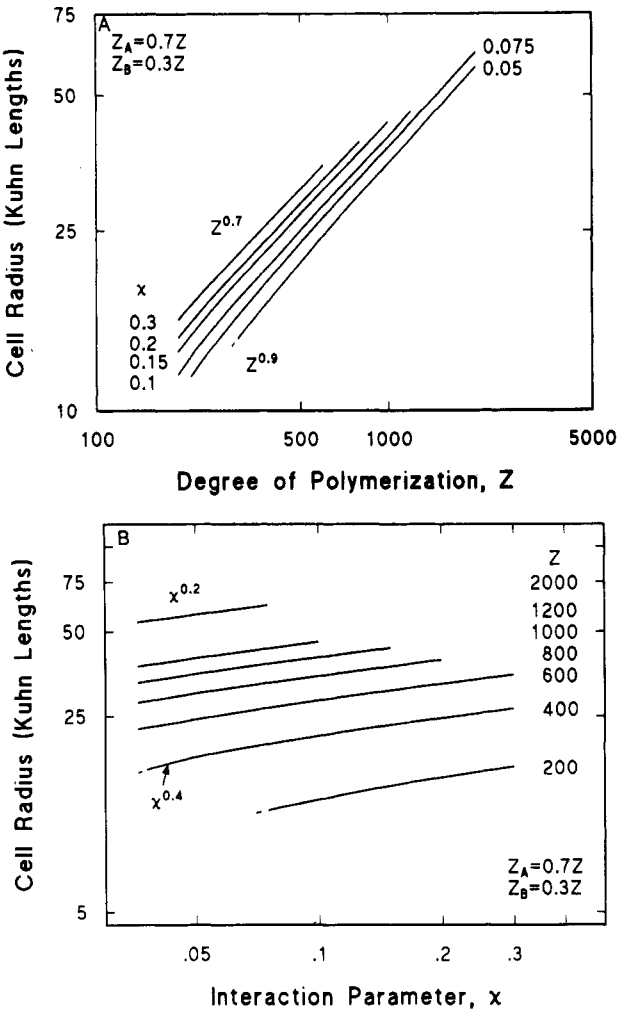

Figure 5. (A) Equilibrium unit cell radius R as a function of Z for asymmetric copolymers with $f_A = 0.7$, for the cylindrical structure. (B) Equilibrium unit cell radius R as a function of χ for the same system. All results represent values calculated from the full self-consistent theory. The solid lines correspond to systems for which the cylinders have the lowest free energy, whereas the dashed line segments represent regions where the spheres are predicted to be stable relative to the cylinders, and are extended to the MST. The line for $\chi = 0.075$ terminates on the left at the C ↔ S transition. The other lines terminate before the C ↔ S transition is reached.

can be expressed approximately as

$$R/b \propto \chi^p Z^q \tag{21}$$

where R is the repeat distance for the layered structure or the radius of the approximate unit cell as described in section 2 and b is the Kuhn length. In Appendix II we show that if we use eq 21, then the powers are related by

$$q = p + {}^1/_2 \tag{22}$$

so we can rewrite eq 21 as

$$R/b \propto [\chi Z]^p Z^{1/2} \tag{23}$$

independent of whether the system is in the weak or strong segregation regime, and for all three structures.

Figure 4 shows d vs Z and χ for symmetric copolymers in the lamellar structure. The solid curves in this figure resulted from full self-consistent calculations. However, in this case the amplitudes of the density variations and the free energy vanish continuously as the MST is approached, making it difficult to calculate ΔF_L and locate its minimum with sufficient precision for this figure. However, Leibler's RPA theory gives the limiting value for d in this case,[1] and so we used it to extrapolate three of these curves to the MST. These extrapolations are shown by dotted line segments. As found for the copolymer/neutral solvent case, the effective powers are largest in the weak segregation regime. In strong segregation, they are given by $p \simeq 0.2$ and $q \simeq 0.7$, but as the system approaches the MST, they approach $p = {}^1/_2$ and $q = 1$.

For the spheres and cylinders, the values $p = 0.2$ and $q = 0.7$ were found again for the strong segregation regime. However, the changes in their values in the weak segregation regime were smaller. In Figure 5 we consider copolymers with $f_A = 0.7$ forming cylinders. As these systems approached the C ↔ S transition, the powers increased to $p \simeq 0.4$ and $q \simeq 0.9$. For smaller values of χZ there is a region in which $\Delta F_S < \Delta F_C < 0$, indicating that the cylinders are metastable. Results for this region are shown by the dashed line segments. In this region, the powers increased further, but to values which were slightly less than those reached for the symmetric copolymers, to $p \simeq 0.45$ and $q \simeq 0.95$.

The case of highly asymmetric copolymers, $f_A = 0.9$, is shown in Figure 6. In this case, the free energy is relatively insensitive to the lattice constant, particularly near the MST. This prevented us from calculating the equilibrium lattice constant very close to the MST with sufficient

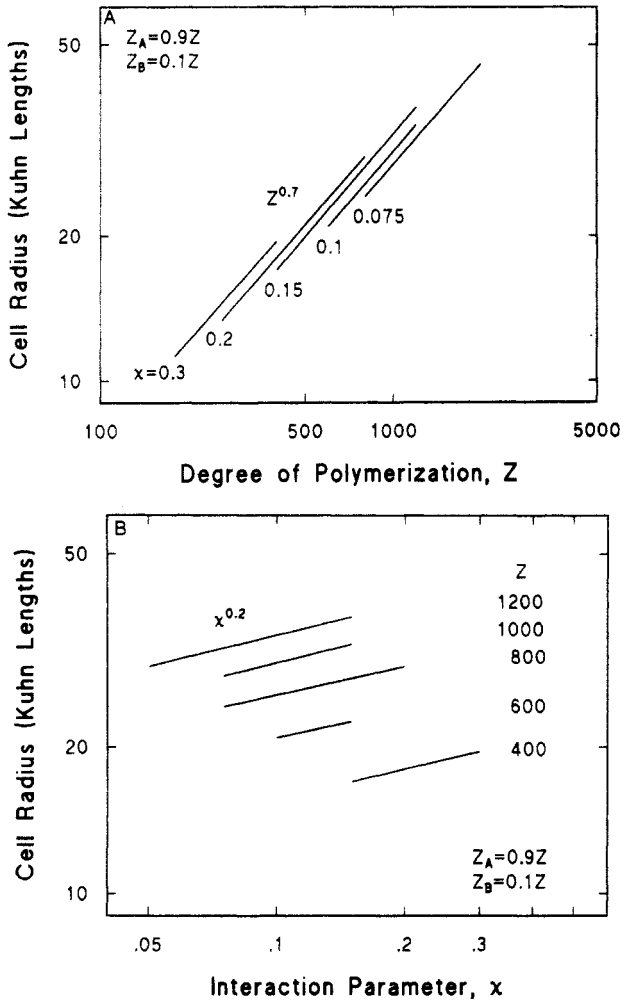

Figure 6. (A) Equilibrium unit cell radius R as a function of Z for asymmetric copolymers with $f_A = 0.9$, for the spherical structure. (B) Equilibrium unit cell radius R as a function of χ for the same system. All results represent values calculated from the full self-consistent theory, and systems in which spheres are predicted to be stable. All lines terminate on the left before the MST is reached.

precision for this figure. Furthermore, it is clear from the above discussion that, unlike the symmetric copolymer case, the RPA weak segregation theory would not necessarily give the correct limit for this system. For these reasons, we terminated these curves at $\chi Z \geq 52$, which compares with the MST value of $\chi Z \simeq 48$ for this value of f_A. Within these limitations, we detected no significant variation in the exponents from their strong segregation values, finding $p = 0.2$ and $q = 0.7$. However, we cannot rule out the possibility of a small increase near the MST. On the other hand, as we shall see below, the nature of the density profiles in this region is consistent with there being no change in these values.

These results are consistent with other work in the appropriate cases. For the strong segregation regime, Helfand and Wasserman's self-consistent theory with the narrow interphase approximation gave $p = 1/7 \simeq 0.14$ and $q = 9/14 \simeq 0.64$.[14] Very recently, Shull studied the lamellar structure of copolymers using self-consistent mean field theory, covering the weak to strong segregation regimes.[30] His formalism is very similar to the one used here, with the primary difference being the method used to incorporate the incompressibility. He found values of $p \simeq 0.17$ and $q \simeq 0.67$ for the strong segregation regime. Both of these sets of results are in reasonable agreement with the current values $p \simeq 0.2$ and $q \simeq 0.7$. For the weak segregation theory, Shull found increases to $p \simeq 0.45$ and $q = 0.95$ for symmetric copolymers, very similar to our values of 0.5 and 1.

Mayes and Olvera de la Cruz treated the weak segregation regime using mean field theory with a fourth-order expansion of the free energy, but keeping four harmonics for each density.[18] They showed results for the lamellar structure for $f_A = 0.4$ and the cylindrical structure for $f_A = 0.3$. For the unit cell, they calculated x^* as a function of χZ, where $x^* \propto Z/R^2$ with the proportionality constant depending on the structure. In both cases, for χZ sufficiently close to the MST, x^* decreased linearly with χZ, with an initial slope defined by

$$\alpha \equiv \Delta x^*/\Delta(\chi Z) \tag{24}$$

They obtained $\alpha \simeq -0.37$ for the lamellar case, and $\alpha \simeq -0.27$ for the cylindrical case. The linear dependence held over the ranges $11.3 \lesssim \chi Z \lesssim 13$ in the first case and $14.3 \lesssim \chi Z \lesssim 16$ in the second, where the lower limit of each of these intervals corresponds to the MST. They compared their result of -0.37 with the value $\alpha \simeq -0.3$ extracted from related experiments.

We can make a quantitative comparison with these results by noting that an assumed power law dependence for the unit cell radius, eq 23, implies

$$x^* \propto 1/(\chi Z)^{2p} \tag{25}$$

where the proportionality constant depends on the structure and f_A. This can be differentiated to give

$$\alpha = -2p\frac{x_0^*}{(\chi Z)_0} \tag{26}$$

for the slope at the MST, where x_0^* and $(\chi Z)_0$ are the values of x^* and χZ at the MST. For $f_A = 0.5$, $x_0^* \simeq 3.78$ and $(\chi Z)_0 \simeq 10.5$, and using our result $p = 1/2$ yields for the initial slope a value $\alpha \simeq -0.36$. Similarly, for $f_A = 0.7$ and 0.9, our results yield $\alpha \simeq -0.27$ and -0.06, respectively. The value for $f_A = 0.7$ can be compared directly with that of Mayes and Olvera de la Cruz; both methods gave $\alpha \simeq -0.27$.

In spite of the good agreement for the lattice parameters, there is an important difference in the phase diagrams calculated by the full self-consistent theory and by a fourth-order expansion. In particular, for those values of χZ for which Mayes and Olvera de la Cruz found linear dependences for x^* on χZ, the fully self-consistent theory predicts that the structures which they assumed are not the equilibrium ones.

Banaszak and Whitmore used an approach which is similar to that of Mayes and Olvera de la Cruz for the lamellar structure of copolymers and copolymer/homopolymer blends.[31] For copolymers, they found $p \simeq 0.5$ and $q \simeq 1$ very near the MST, in agreement with the current results.

The above summary also indicates that, in all cases, the results obeyed the scaling law, eq 22. Furthermore, those for copolymer/solvent blends also obeyed it, and in fact the values for p and q were very similar to those found numerically for the lamellar structure for copolymers.[27,29] These results follow analytically from the theory if the dilution approximation is made.

3.4. Density Profiles. Each self-consistent calculation produced an accompanying set of density profiles, $\phi_A(r)$ and $\phi_B(r)$. It follows from the discussion in Appendix I that when the length scales are normalized to the equilibrium unit cell size, the density profiles for each structure depend on only χr_C, f_A, and ϵ, or in the present case on only χZ and f_A. Figures 7–9 show two sets of profiles for each structure.

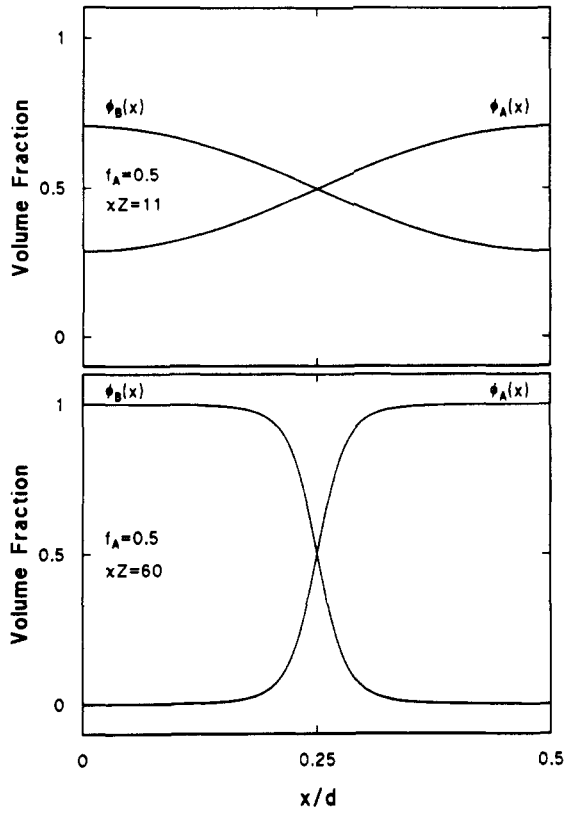

Figure 7. Calculated density profiles $\phi_A(x)$ and $\phi_B(x)$ for symmetric copolymers in the lamellar structure. The top panel corresponds to the weak segregation regime with $\chi Z = 11$, whereas the bottom panel corresponds to the strong segregation regime with $\chi Z = 60$.

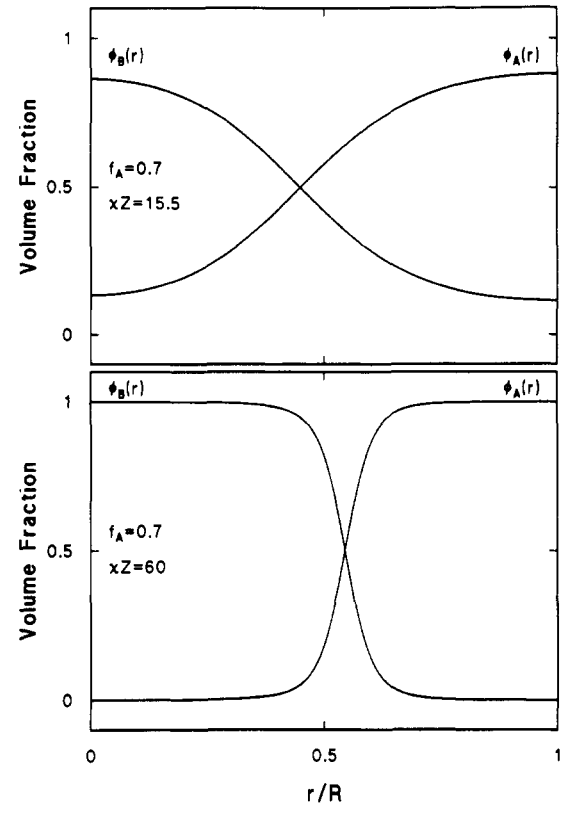

Figure 8. Calculated density profiles $\phi_A(r)$ and $\phi_B(r)$ for asymmetric copolymers in the cylindrical structure. For this geometry, the proportion of each component a distance r from the origin is proportional to $2\pi r\phi_p(r)$. The top panel corresponds to a system with $\chi Z = 12$, and so is close to the MST. It is also essentially at the L ↔ C microphase boundary. For the bottom panel, $\chi Z = 60$ and the system is strongly segregated, and not very close to any microphase boundary.

Figure 7 is for symmetric copolymers in the lamellar structure. For the top panel, $\chi Z = 11$ which is very near the MST at $\chi Z = 10.5$. Qualitatively, the two profiles $\phi_A(r)$ and $\phi_B(r)$ are given by cosine-like variations about their mean values, but even for this modest value of χZ, the amplitudes of the variations are approaching half of the mean values. Decreasing χZ toward 10.5 causes these amplitudes to decrease smoothly to zero. Conversely, increasing χZ causes them to increase, and the profiles to begin to flatten within each subdomain. For $\chi Z \gtrsim 15$, each local volume fraction is essentially unity at the center of one subdomain and zero in the other. As χZ is further increased, the interfaces sharpen and the local volume fractions remain one or zero over a progressively larger distance. The progression is very similar to that for the copolymer/neutral solvent blends, illustrated in detail in ref 27. For this paper we exhibit, in the lower panel of Figure 7, a system with $\chi Z = 60$, which has reached well into the strongly segregated regime.

The profiles for the other structures exhibit qualitatively different behavior in the weak segregation regime, due to the fact that for asymmetric copolymers the transitions are first order. The top panel of Figure 8 shows the density profiles for asymmetric copolymers with $f_A = 0.7$ and $\chi Z = 15.5$, in the cylindrical morphology. This system is close to the MST which is at $\chi Z \simeq 14$ for these copolymers, and is virtually at the C ↔ S transition. Even so, the amplitude of the variation of each density is approximately 70% of the overall values. The lower panel corresponds to the cylindrical morphology in the strong segregation regime, with $\chi Z = 60$ as in the lower panel of Figure 7. Again the shape is characteristic of the strong segregation regime, being one or zero within each subdomain, with a relatively narrow interphase region.

Finally, Figure 9 shows density profiles for spheres, using modestly asymmetric copolymers with $f_A = 0.636$ in the upper panel and highly asymmetric ones with $f_A = 0.9$ in the lower one. In both cases the systems are close to the MST. The first corresponds to a system with $\chi Z = 12$, and is right at the MST. As in the upper panel of Figure 8, the amplitudes of the density variations are on the order of 50% of the overall values, and the shapes are typical of the weak segregation regime. For the system illustrated in the lower panel, $\chi Z = 80$ but the system is near the MST because of the high degree of asymmetry of these molecules. The RPA weak segregation theory predicts that the MST for this value of χZ is just to the right of this system on the microphase diagram at $f_A \simeq 0.91$, and the current calculation places it at $f_A \simeq 0.93$. The most interesting aspect of this panel is that, in spite of the system's proximity to the MST, the density profiles are typical of those normally associated with the strong segregation regime, such as in the lower panels of Figures 7 and 8, with broad regions in which each is zero or unity, and a relatively narrow interphase region.

The calculated density profiles can be compared with some earlier work. The top panel of Figure 7, for which $\chi Z = 11$, is very similar to the top panel of Figure 3 of Shull[30] which shows a density profile for the layered structure for symmetric copolymers with $\chi Z = 12$. The primary difference is a different amplitude, as one would expect. He found that for $\chi Z = 14$, the maximum has nearly reached unity, consistent with our results.

We can also compare the self-consistent calculations with approaches based on fourth-order expansions, using as a model the lamellar structure with $f_A = 0.4$. For $\chi Z = 12$, the self-consistent calculations gave $\phi_A(x)$ varying

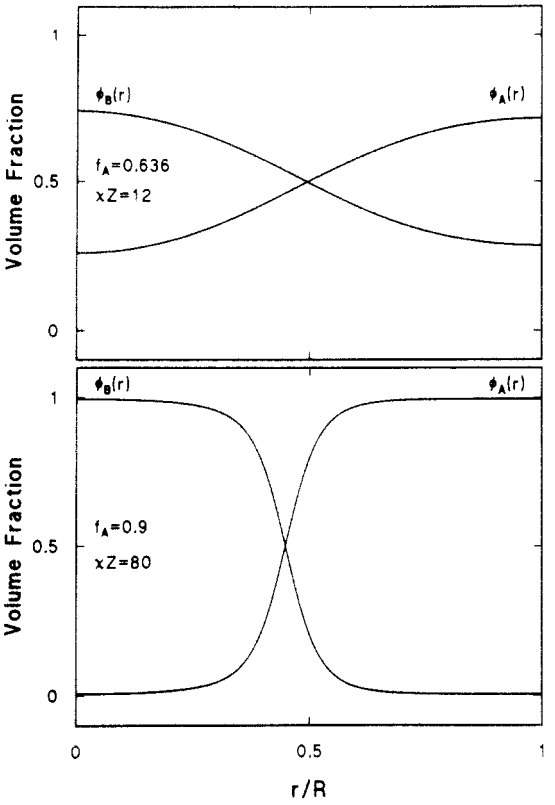

Figure 9. Calculated density profiles $\phi_A(r)$ and $\phi_B(r)$ for asymmetric copolymers in the spherical structure. For this geometry, the proportion of each component a distance r from the origin is proportional to $4\pi r^2\phi_p(r)$. The top panel corresponds to a system with $\chi Z = 12$ and is virtually at the MST. The profiles are qualitatively cosine-like, with amplitudes which are approximately 50% of the average values. For the bottom panel, the copolymers are highly asymmetric with $f_A = 0.9$ as indicated, and $\chi Z = 80$. Nonetheless, this case is also close to the MST, which occurs at $f_A = 0.93$ for this value of χZ. Even this close to the MST, the profiles in this case resemble those normally associated with the strong segregation regime.

from about 0.19 to 0.65. Banaszak and Whitmore found virtually the same extrema, with $\phi_A(x)$ varying from about 0.18 to 0.66. Mayes and Olvera de la Cruz found somewhat smaller variations, with $\phi_A(x)$ ranging from about 0.28 to 0.53. For the same case except for χZ increased further to 13, the self-consistent calculations give $\phi_A(x)$ ranging from about 0.13 to 0.76; again, Mayes and Olvera de la Cruz found a smaller variation, from about 0.22 to 0.62 for this case.

4. Discussion and Summary

We have examined the microphases of diblock copolymers using self-consistent mean field theory, assuming the interactions can be modeled by a simple Flory χ parameter. We considered three microstructures, layers, cylinders, and spheres, exhibiting the microphase diagram, lattice constants, and sample density profiles, and their dependence on total and block degrees of polymerization and on χ. We did not consider more complex structures such as the OBDD or the ones newly discovered by Almdal et al.[2]

The mean field theory makes two general predictions, which apply to all three structures in both strong and weak segregation regimes.

First, the entire phase diagram is controlled by three quantities, χr_C, f_A, and $\epsilon \equiv (\rho_{0B}b_B^2)/(\rho_{0A}b_A^2)$. This is a generalization of Leibler's result for the weak segregation limit that, for the case $\rho_{0A} = \rho_{0B}$ and $b_A = b_B$, it is controlled by only χZ and f_A. The relevance of the third parameter, ϵ, is consistent with a similar suggestion of Almdal et al.[2]

The second prediction is that if the scaling of the size of the lattice parameter is expressed as $R/b \propto \chi^p r_C^q$, then $q = p + 1/2$. This was found to be satisfied by the results of all previous mean field calculations. It is difficult, however, to compare it with experiments, since they directly give d vs T, rather than d vs χ. For example, as discussed in ref 27, Hashimoto and co-workers[32-36] found that for a series of PS-b-PI copolymers, with and without a nonselective solvent DOP, the scaling of d was approximately $d \propto [\bar{\phi}_c/T]^{1/3}Z^{2/3}$. A full test of eq 22 would require a precise measurement of χ as a function of T.

For the numerical work, we restricted ourselves to the case $\epsilon = 1$ and presented results explicitly for the case $\rho_{0A} = \rho_{0B}$, pointing out that they would also apply to other systems with $\epsilon = 1$ through the replacement of Z with r_C. The study of specific systems such as PS-b-PBD or PS-b-PI is ongoing.

The first numerical results constituted the microphase diagram. In agreement with the RPA theory of Leibler, for symmetric copolymers we found the MST to be a second-order transition to layers, occurring at $\chi Z = 10.5$, and that for any other copolymers the MST is to spheres. However, we found that the microphase boundaries curved rather quickly toward the values for the strong segregation regime. For a fixed χZ, the regions of cylinders and spheres were significantly wider than those predicted by all previous theories of block copolymers for the weak segregation regime. Furthermore, particularly for highly asymmetric copolymers, the MST was shifted to smaller values of χZ, and the region of the phase diagram near the MST differed through the presence of much wider S regions. In the strong segregation regime, the phase boundaries agreed with those predicted for this system using the narrow interphase approximation of Helfand and co-workers.[10]

For fixed $f_A \neq 0.5$, the theory predicts a sequence of phases with increasing χZ. For example, for $f_A = 0.65$, the first ordered phase is S, which very quickly gives way to C which is predicted to persist over a range $13 \lesssim \chi Z \lesssim 25$, at which point it in turn gives way to L. However, for all values of f_A for which layers are predicted to occur, the S region is predicted to be extremely small. Furthermore, studies which incorporate fluctuation effects have implied that these very narrow S regions for nearly symmetric copolymers may be artifacts of mean field theory.[17] Taken together, these theoretical results suggest that, at least for molecules characterized by $\epsilon \simeq 1$, in practice no copolymers would exhibit more than two of these morphologies: symmetric copolymers would form layers, copolymers with $0.35 \lesssim f_A \lesssim 0.65$ could form layers or cylinders but not spheres, and more asymmetric copolymers could form spheres or cylinders but not layers.

These results are in qualitative agreement with the recent experiments of Almdal et al. on PEP–PEE with $f_{PEP} \simeq 0.65$.[2] They found a sequence of microphases, from H at high temperature through two intermediate phases to L at low temperature. The high- and low-temperature phases agree with the current calculations, as does the existence of a sequence of phases for $f_A \simeq 0.65$. However, the two intermediate phases differed from the two possibilities (C and S) modeled here.

We found that the domain sizes scaled as $R/b \propto \chi^{0.2}Z^{0.7}$ in the strong segregation regime, but as the systems approached the MST, the values of the powers increased. For symmetric copolymers the transition is continuous,

and the exponents reached $p \simeq 1/2$ and $q \simeq 1$. For the asymmetric copolymers, they increased, but not as much. For the case of $f_A = 0.7$, they reached $p \simeq 0.4$ and $q \simeq 0.9$ for stable cylinders, and $p \simeq 0.45$ and $q \simeq 0.95$ for metastable cylinders. For the highly asymmetric copolymers with $f_A = 0.9$ in the spherical morphology, we detected no increase in these values, although the precision of our numerical results for this case does not rule out a small increase. These results are in reasonable agreement with those of Helfand and Wasserman[14] in the strong segregation limit, of Shull[30] for layers in strong and weak segregation, and of Mayes and Olvera de la Cruz[18] for layers and cylinders and Banaszak and Whitmore[31] for layers in weak segregation. However, for the ranges of χZ for which the procedure of Mayes and Olvera de la Cruz appeared to be applicable, the full self-consistent theory indicated that the structures which they assumed were not the equilibrium morphologies.

The nature of the calculated density profiles correlated with these results. For all cases, in the strong segregation regime each of $\phi_A(r)$ and $\phi_B(r)$ was virtually unity throughout one subdomain, decreased smoothly to zero through a relatively narrow interphase region, and remained such throughout the other subdomain. For systems in progressively weaker segregation regimes, the interphase region began to widen and the regions of constant density to narrow. As the MST was approached, the behavior depended on the system. For symmetric copolymers, the two profiles relaxed toward cosine-like functions, with amplitudes which decreased continuously to zero at the transition. As this happened, the powers approached $p = 1/2$ and $q = 1$. For asymmetric copolymers, the order–disorder transition was discontinuous. In these cases, the degree to which the profiles relaxed toward cosine-like functions, and the maximum values of p and q, depended on the asymmetry. For modestly asymmetric copolymers, the variations in the densities became quite cosine-like, their amplitudes remained rather large, and p and q nearly reached one-half and unity. The case of highly asymmetric copolymers was qualitatively different. Even when close to the MST, the density profiles were similar to those normally associated with the strong segregation regime. This was illustrated in the lower panel of Figure 9. There was, correspondingly, no detectable increase in the values of the exponents from their strong segregation regime values.

A general conclusion of these calculations is that understanding these systems probably requires taking into account the actual shapes of these profiles rather than relying on expansions involving a few wavenumbers, and using more than a fourth-order expansion for the free energy. This applies particularly to the identification of the microphase boundaries, since the differences between the free energies of the competing morphologies is so small. It is also likely the case that a full understanding of them requires the inclusion of fluctuation effects[17] as well.

Finally, we note that the results found here agree closely with earlier work on copolymer/neutral solvent systems, if we make the identification of $\chi_{eff} = \bar{\phi}_c\chi$. This has two implications. First, since the earlier work was done with the finite range parameter σ set equal to a Kuhn length rather than zero as in this paper, it implies that the effect of finite σ is very small. Second, within mean field theory, the dominant effect of a nonselective solvent can be incorporated via a simple reduction of χ to an effective value, which is consistent with the dilution approximation. This approach does not include swelling by a good solvent, but at least in strong segregation, that seems to have little effect on the phase diagram.[21]

Acknowledgment. This work was supported in part by the Natural Sciences and Engineering Research Council of Canada.

Appendix I: Functional Dependence of the Phase Diagram

In principle, the equilibrium morphology of a system of linear, monodisperse block copolymers could depend on eight quantities: the total degree of polymerization, the two Kuhn statistical lengths, the two pure component densities, the overall volume fraction of one component, the interaction parameter χ, and the range of the interaction. In this appendix, we show that, for $\sigma = 0$, the phase diagram is determined by only three quantities.

We need to carry out the self-consistent calculation for each structure at a given lattice constant R. Approximating the unit cells for two- and three-dimensional ordering by cylinders and spheres, respectively, we can rescale all lengths by $r \to r/R$, and the "time" scale by $\tau \to \tau/Z_p$, for each block. The diffusion equation, eq 3, becomes

$$\left[-\frac{b_p^2}{6R^2}\nabla^2 + \omega_p(\mathbf{r})\right]Q_p(\mathbf{r}, \tau|\mathbf{r}') = -\frac{1}{Z_p}\frac{\partial}{\partial\tau}Q_p(\mathbf{r}, \tau|\mathbf{r}') \quad (27)$$

If we multiply this by $r_C\rho_{0p}/\rho_0$, then it becomes

$$[-\epsilon_p\beta\nabla^2 + \omega_p'(\mathbf{r})]Q_p(\mathbf{r}, \tau|\mathbf{r}') = -\frac{1}{f_p}\frac{\partial}{\partial\tau}Q_p(\mathbf{r}, \tau|\mathbf{r}') \quad (28)$$

where

$$\beta = \frac{r_C\rho_{0A}b_A^2}{6\rho_0R^2} \quad (29)$$

$$\epsilon_p = \frac{\rho_{0p}b_p^2}{\rho_{0A}b_A^2} \quad (30)$$

and the potentials $\omega_p'(\mathbf{r})$ can be written

$$\omega_A'(\mathbf{r}) = \chi r_C[\phi_B(\mathbf{r}) - \bar{\phi}_B] + \eta'(\mathbf{r}) \quad (31)$$

$$\omega_B'(\mathbf{r}) = \chi r_C[\phi_A(\mathbf{r}) - \bar{\phi}_A] + \eta'(\mathbf{r}) \quad (32)$$

where $\eta'(\mathbf{r}) = \eta(\mathbf{r})r_C$. Since $\epsilon_A = 1$, we can simplify the notation by denoting $\epsilon_B \equiv \epsilon$.

The convolutions for the local volume fractions are modified accordingly; e.g., eq 5 for $\phi_A(\mathbf{r})$ can be written as

$$\phi_A(r) = \frac{\bar{\phi}_A V}{\mathcal{Q}'_C}\int_0^1 d\tau\, q_A(r, \tau)\, \tilde{q}_A(r, 1-\tau) \quad (33)$$

where

$$\tilde{q}_A(r, 1-\tau) = \int d\mathbf{r}'\, Q_A(\mathbf{r}, 1-\tau|\mathbf{r}')\, q_B(\mathbf{r}', 1) \quad (34)$$

which depends only on $r = |\mathbf{r}|$, and

$$\frac{\mathcal{Q}'_C}{V} = \frac{m}{\alpha_m(1)}\int_0^1 \alpha_m(r)\, dr\, q_A(r, 1)\, q_B(r, 1) \quad (35)$$

where $m = 1$, 2, or 3 for layers, cylinders, or spheres, respectively, and $\alpha_1(r) = 1$, $\alpha_2(r) = 2\pi r$, and $\alpha_3(r) = 4\pi r^2$.

Equations 28–35 form a new set of self-consistent equations. When they are solved, the resulting free energy

can be expressed as

$$\frac{\Delta F}{\rho_0 k_B T V} = \frac{1}{r_C}\left[\frac{m}{\alpha_m(1)}\int_0^1 \alpha_m(r)\,dr\,\{\chi r_C \phi_A(r)\,\phi_B(r) - \omega_A'(r)\,\phi_A(r) - \omega_B'(r)\,\phi_B(r)\} - \ln\left(\frac{Q_C'}{V}\right)\right] \quad (36)$$

Equations 28–35 depend on only β, f_A, ϵ, and the product χr_C (since $f_B = 1 - f_A$). The free energy, eq 36, depends on r_C as well, but only as a prefactor, and so this has no effect on the equilibrium morphology. In principle, these equations also depend on σ, which we have taken to be zero, but this is a weak dependence. Thus, there are four controlling quantities, β, f_A, ϵ, and χr_C.

The minimization of the free energy with respect to the lattice constant can be formulated as the minimization of $r_C \Delta F$ with respect to β:

$$\frac{\partial}{\partial \beta}\left(\frac{r_C \Delta F}{\rho_0 k_B T V}\right) = 0 \quad (37)$$

This represents a holonomic constraint which reduces the number of independent variables to three. Since the blend is characterized by the three quantities χr_C, f_A, and ϵ, it is convenient to think of eq 37 as specifying the equilibrium value of β as a function of these three variables; i.e.

$$\beta_{eq} = \beta_{eq}(\chi r_C, f_A, \epsilon) \quad (38)$$

The equilibrium morphology is also a function of these three remaining variables.

Appendix II: Scaling Laws for Equilibrium Lattice Constants

Equation 37 of Appendix I defines an implicit function for the equilibrium value of β as a function of ϵ, f_A, and χr_C. If we assume that the equilibrium value of R obeys

$$R \propto \chi^p r_C^q \quad (39)$$

then substituting this into the definition of β, eq 29, gives

$$\beta_{eq} \propto \frac{r_C \rho_{0A} b_A^2}{6\rho_0 \chi^{2p} r_C^{2q}} = \frac{\rho_{0A} b_A^2}{6\rho_0}(\chi r_C)^{-2p} r_C^{1+2p-2q} \quad (40)$$

However, since the form of eq 38 implies that β_{eq} depends on r_C only through the product χr_C, we must have $1 + 2p - 2q = 0$, and so at equilibrium

$$q = p + {}^1/_2$$
$$R \propto \chi^p r_C^{p+1/2} \quad (41)$$

As discussed in section 3, this is consistent with theoretical work using mean field theory in both weak and strong segregation regimes.

References and Notes

(1) Leibler, L. *Macromolecules* **1980**, *13*, 1602.
(2) Almdal, K.; Koppi, K. A.; Bates, F. S.; Mortensen, K. *Macromolecules* **1992**, *25*, 1743.
(3) Hasegawa, H.; Tanaka, H.; Yamasaki, K.; Hashimoto, T. *Macromolecules* **1987**, *20*, 1651.
(4) Thomas, E. L.; Alward, D. B.; Kinning, D. L.; Martin, D. L.; Handlin, D. L., Jr.; Fetters, L. J. *Macromolecules* **1986**, *19*, 2197.
(5) Tanaka, H.; Sakurai, S.; Hashimoto, T.; Whitmore, M. D. *Polymer* **1992**, *33*, 1006.
(6) Brandrup, J., Immergut, E. H., Eds. *Polymer Handbook*, 2nd ed.; Interscience: New York, 1975.
(7) Bonner, C. C.; Prausnitz, J. M. *AIChE J.* **1973**, *19*, 943.
(8) Höcker, H.; Blake, C. J.; Flory, P. J. *Trans. Faraday Soc.* **1971**, *67*, 2251.
(9) Kruse, R. L. In *Copolymers, Polyblends and Composites*; Platzer, N. A. J., Ed.; American Chemical Society: Washington, DC, 1975; p 141.
(10) Helfand, E.; Wasserman, Z. R. In *Developments in Block Copolymers*; Goodman, I., Ed.; Elsevier: New York, 1982; Vol. 1.
(11) Helfand, E. In *Recent Advances in Polymer Blends, Grafts and Blocks*; Sperling, L. H., Ed.; Plenum: New York, 1974.
(12) Helfand, E. *Macromolecules* **1975**, *8*, 552.
(13) Helfand, E. *J. Chem. Phys.* **1975**, *62*, 999.
(14) Helfand, E.; Wasserman, Z. R. *Macromolecules* **1976**, *9*, 879.
(15) Helfand, E.; Wasserman, Z. R. *Macromolecules* **1978**, *11*, 960.
(16) Helfand, E.; Wasserman, Z. R. *Macromolecules* **1980**, *13*, 994.
(17) Fredrickson, G. H.; Helfand, E. *J. Chem. Phys.* **1987**, *87*, 697.
(18) Mayes, A. M.; Olvera de la Cruz, M. *Macromolecules* **1991**, *24*, 3975.
(19) Olvera de la Cruz, M. *Phys. Rev. Lett.* **1991**, *67*, 85.
(20) Mayes, A. M.; Olvera de la Cruz, M. *J. Chem. Phys.* **1991**, *6*, 4670.
(21) Birshtein, T. M.; Zhulina, E. B. *Polymer* **1990**, *31*, 1312.
(22) Noolandi, J.; Hong, K. M. *Ferroelectrics* **1980**, *30*, 117.
(23) Hong, K. M.; Noolandi, J. *Macromolecules* **1981**, *14*, 727.
(24) Vilgis, T.; Noolandi, J. *Macromolecules* **1990**, *23*, 2941.
(25) Shull, K. R.; Kramer, E. J. *Macromolecules* **1990**, *23*, 4769.
(26) Whitmore, M. D.; Vavasour, J. D. *Macromolecules* **1992**, *25*, 2041.
(27) Whitmore, M. D.; Noolandi, J. *J. Chem. Phys.* **1990**, *93*, 2946.
(28) Whitmore, M. D.; Noolandi, J. *Macromolecules* **1988**, *21*, 1482.
(29) Banaszak, M.; Whitmore, M. D.; *Macromolecules* **1992**, *25*, 249.
(30) Shull, K. R. *Macromolecules* **1992**, *25*, 2122.
(31) Banaszak, M.; Whitmore, M. D. *Macromolecules* **1992**, *25*, 2757.
(32) Hashimoto, T.; Todo, A.; Itoi, H.; Kawai, H. *Macromolecules* **1977**, *10*, 337.
(33) Hashimoto, T.; Shibayama, M.; Kawai, H. *Macromolecules* **1980**, *13*, 1237.
(34) Hashimoto, T.; Shibayama, M.; Kawai, H. *Macromolecules* **1983**, *16*, 1093.
(35) Shibayama, M.; Hashimoto, T.; Hasegawa, H.; Kawai, H. *Macromolecules* **1983**, *16*, 1427.
(36) Shibayama, M.; Hashimoto, T.; Kawai, H. *Macromolecules* **1983**, *16*, 1434.